HPro: A NLO Monte-Carlo for Higgs production via gluon fusion with finite heavy quark masses

JHEP10(2009)068

(http://iopscience.iop.org/1126-6708/2009/10/068)

Published by IOP Publishing for SISSA

Received: *July 15, 2009*
Accepted: *September 29, 2009*
Published: *October 26, 2009*

HPro: A NLO Monte-Carlo for Higgs production via gluon fusion with finite heavy quark masses

Charalampos Anastasiou, Stefan Bucherer and Zoltan Kunszt

Institute for Theoretical Physics, ETH Zurich,
8093 Zurich, Switzerland
E-mail: babis@phys.ethz.ch, stefabu@itp.phys.ethz.ch, kunszt@itp.phys.ethz.ch

Abstract: We compute fully differential next-to-leading order QCD cross-sections for Higgs boson production via gluon fusion in the Standard Model. We maintain the full dependence of the cross-sections on the top and bottom quark mass. We find that finite quark mass effects are important given the achieved precision of QCD predictions for gluon fusion. Our Monte-Carlo program `HPro` can correct existing NNLO fully differential calculations, which employ the approximation of an infinitely heavy top and a vanishing bottom quark Yukawa coupling, for heavy quark finite mass effects through NLO.

Keywords: Higgs Physics, NLO Computations

ArXiv ePrint: 0907.2362

doi:10.1088/1126-6708/2009/10/068

JHEP10(2009)068

Contents

JHEP10(2009)068

1 Introduction

QCD radiative effects in the gluon fusion process for the production of Higgs bosons at hadron colliders have been the subject of detailed theoretical investigations in the last two decades. The next-to-leading order QCD corrections to the inclusive cross-section were computed already in the nineties [1–3]. In these works it was shown that QCD perturbative corrections are substantial.

Exact calculations of perturbative corrections in the gluon fusion process, such as in ref. [3], are technically involved due to the presence of massive quark loops already at the leading order. With these pioneering NLO computations, the quality of the simplifying approximation of an infinitely heavy top quark and vanishing Yukawa couplings for all other quarks could be assessed.

Such an approximation is indispensable for computing QCD perturbative corrections beyond NLO. Next-to-next-to-leading order QCD corrections for the $gg \to H$ inclusive cross-section were computed in Refs [4–6]. NNLO corrections, within the same approximation, for fully differential cross-sections were computed in Refs [7–9] and in Refs [10, 11].

The theoretical uncertainty due to scale variations of NNLO inclusive and differential cross-sections is by now remarkably small. While existing tools, such as `HIGLU` [12] can be used to correct the predictions for the total cross-section for finite quark-mass effects through NLO, fully differential cross-sections for the Higgs boson and its decay products cannot be corrected for the same effects with existing tools. We remedy this situation in our publication.

We have written a parton level Monte-Carlo program `HPro` which computes fully differential cross-sections at NLO in QCD while keeping the exact dependence on the finite top and bottom quark mass. `HPro` includes the decays of the Higgs boson to photons and four-lepton final states. It can be used in conjunction with the fully differential NNLO

program FEHiP [8, 9], correcting for finite quark mass effects through NLO. An earlier version of HPro has been used in [13] to estimate the finite bottom mass effects. Later in a similar study [14] these effects have been also accounted for using HIGLU.

We present the calculation method in section 2. In section 3 we use HPro to compute the NLO total cross-section and review the quality of the approximations which are usually made for heavy quark loops in the gluon fusion process. In section 4, we compute for illustration various kinematic distributions and study the effect of finite quark masses to their shape. We present our conclusions in section 5.

JHEP10(2009)068

2 Implementation

The computation of the NLO corrections to the gluon fusion process requires the two-loop $gg \to h$ amplitude. This has been first computed by means of an one-dimensional integral representation derived in ref. [3]. In ref. [15], this result was expressed analytically in terms of harmonic polylogarithms using a "series expansion and matching" method. Independent analytic evaluations of the two-loop amplitude were performed in ref. [16] and in ref. [17].

At NLO also real radiation sub-processes $gg \to gh$, $qg \to qh$ and $q\bar{q} \to gh$ contribute. The corresponding matrix elements have been first computed in ref. [18]. In ref. [19] these matrix elements have been expressed in terms of standard one-loop scalar integrals and helicity amplitudes. We have recomputed these contributions along the lines of ref. [19] and found full agreement. In particular we have also compared to a very recent calculation in ref. [20]. For completeness we present the results in appendix A.

Virtual and real corrections develop singularities which only cancel in their combination and by adding the appropriate collinear counter-term for PDF evolution. In order to obtain an expression suited for numerical integration we apply the FKS subtraction method [21]. Recently this method has been applied in ref. [22] for the matching of NLO Higgs production to shower Monte Carlo in the heavy top mass approximation.

We note that in the case of total cross sections the straightforward application of the FKS subtraction method leads to the same analytic formula for the subtraction terms that has been found in ref. [3]. With appropriate insertion of measurement functions we easily get analytic expressions suited for the calculation of any differential distribution. In practice one might think of the measurement function as a vector valued function with each component being a bin of a certain distribution. There exist implementations of the VEGAS algorithm supporting vector functions, such as the VEGAS routine in the CUBA library [23], which allows to obtain a reliable Monte-Carlo error estimate for each bin. In combination with dedicated decay routines for the diphoton and leptonic final states, this feature enables us to produce various distributions relevant for experimental searches of the Higgs boson, corrected by finite mass effects, as we will demonstrate in the following sections.

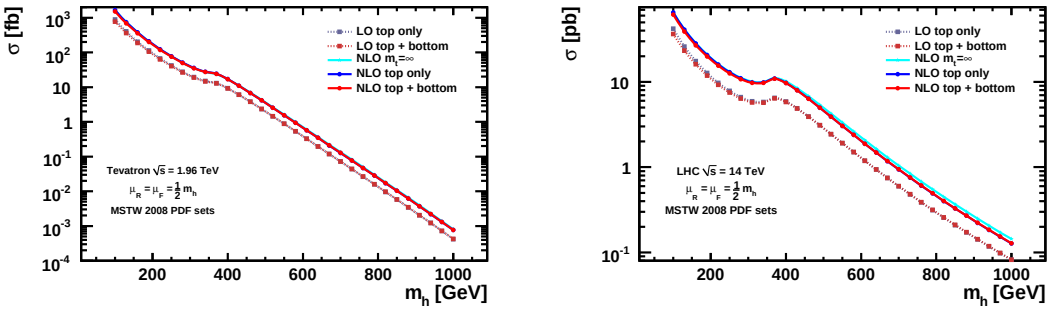

Figure 1. Total Cross-Section at Tevatron and LHC.

3 Total cross-section at NLO

In this section, we revisit the gluon fusion cross-section at NLO. This serves as a check of our Monte-Carlo `HPro` against the predictions of `HIGLU` [12], and to emphasize the importance of finite quark mass effects in Higgs boson production. For the numerical results of this paper we use MSTW 2008 parton distribution functions [24].

We begin our study by revisiting the total cross-section in the LO and NLO approximation as a function of the Higgs boson mass (figure 1). As it is well known [1–3], NLO QCD perturbative corrections are substantial. We note here that the perturbative corrections are slightly smaller with the latest parton densities [24], mainly due to the higher value of α_s used at leading order. We also note that a significant QCD correction is found at NNLO [4–6], which is not included in the results of this article. NNLO corrections stabilize the perturbative expansion and reduce the scale variation to the $\sim 10\%$ level. However, NNLO computations rely on an approximate treatment of heavy quark loops.

In figure 1, we show the effects of different treatments for the heavy quarks. With `HPro`, we compute the exact LO and NLO cross-sections, where all loop diagrams with massive top and bottom quarks are evaluated exactly (we denote with "top+bottom" the corresponding cross-sections in the plots of this paper). An approximation which can be made, is to consider a vanishing bottom Yukawa coupling and to evaluate exactly only the top-quark loops; in our plots, we denote this approximation as "top-only". NNLO computations are performed in what is known as the infinitely heavy top-quark approximation. In the "$m_{\rm top} = \infty$" approximation, the bottom Yukawa coupling is set to zero, and the cross-section at higher orders is estimated by the formula,

$$\sigma^{m_{\rm top}=\infty}_{\rm (N)NLO} = \sigma^{\rm top-only}_{\rm LO} \times \lim_{m_{\rm top}\to\infty} \left(\frac{\sigma^{\rm top-only}_{\rm (N)NLO}}{\sigma^{\rm top-only}_{\rm LO}} \right), \tag{3.1}$$

where bottom quark loops are ignored, and the leading order cross-section is reweighted with the ratio of the cross-sections at higher orders and the leading order in the limit of an infinite top-quark mass. In order to compare the different approximations we introduce

$$\delta X^i = \frac{X^i - X^{m_{\rm top}=\infty}}{X^{m_{\rm top}=\infty}} \tag{3.2}$$

JHEP10(2009)068

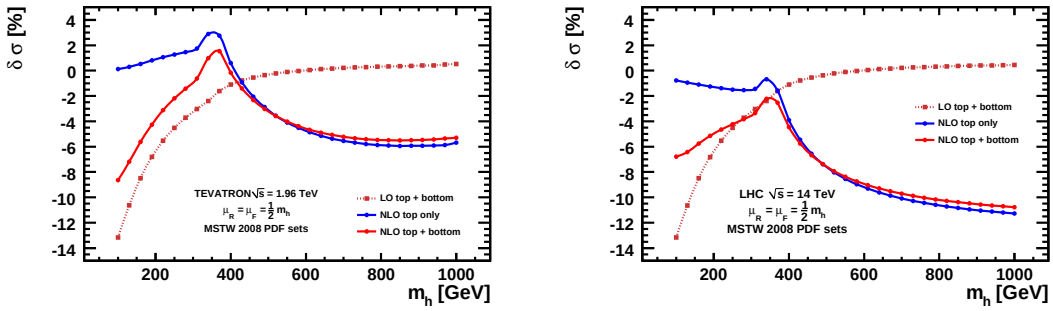

Figure 2. Percent differences of the exact NLO (LO) total cross-section with finite top bottom masses or the NLO (LO) total cross-section with exact top mass effects but zero bottom Yukawa coupling with respect to the usual approximation at Tevatron and the LHC.

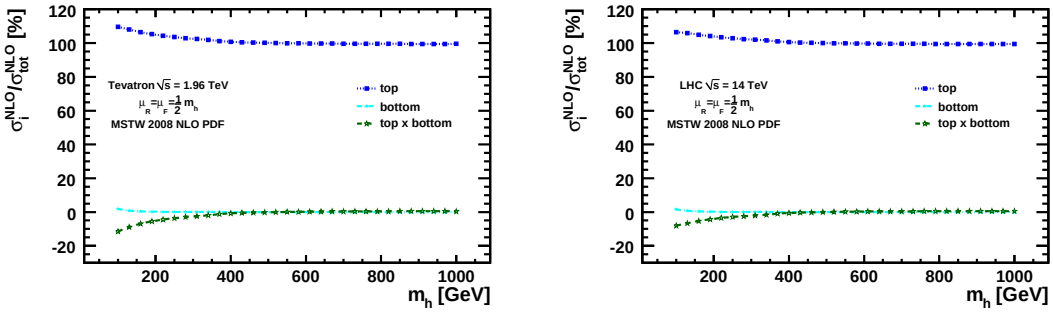

Figure 3. Ratio in percentage of top-only, bottom-only and top-bottom interference components with respect to the total cross-section at NLO, for Tevatron and LHC.

where X is the inclusive cross section or a normalized differential cross section and i is labelling the contribution (top+bottom, top-only, etc.)

In figure 2, we show the cross-section deviations from the $m_{\rm top} = \infty$ approximation of eq. 3.1 when "top-only" (blue) and the complete "top-bottom" mass effects are taken into account. "Top-only" contributions are approximated within a couple of a percent up to the $m_{\rm H} = 2m_{\rm top}$ threshold. However, for a light Higgs boson, bottom quark contributions are important and can reach $\sim -8\%$. It is then important that bottom loops are taken into account for a precise evaluation of the total cross-section [13]. We also observe that the contribution from bottom-quark loops decreases at NLO in comparison to LO.

In figure 3, we show the relative contributions to the NLO total cross-section from top-quark loops only, bottom quark-loops only, and from the interference of top and bottom loops. Top-only contributions are dominant, while bottom-only contributions are negligible over the whole Higgs mass range. Top-bottom interference terms are important at the few percent level and are negative for a light Higgs boson. It should be noted that the relative importance of the three contributions for a heavy Higgs boson or a pseudo-scalar Higgs boson in the MSSM may be drastically different than in the Standard Model [25].

The magnitude of QCD corrections depends strongly on the mass value of the heavy quark in the loops if we use the pole mass for the $q\bar{q}H$ coupling. In figure 4 we consider the

JHEP10(2009)068

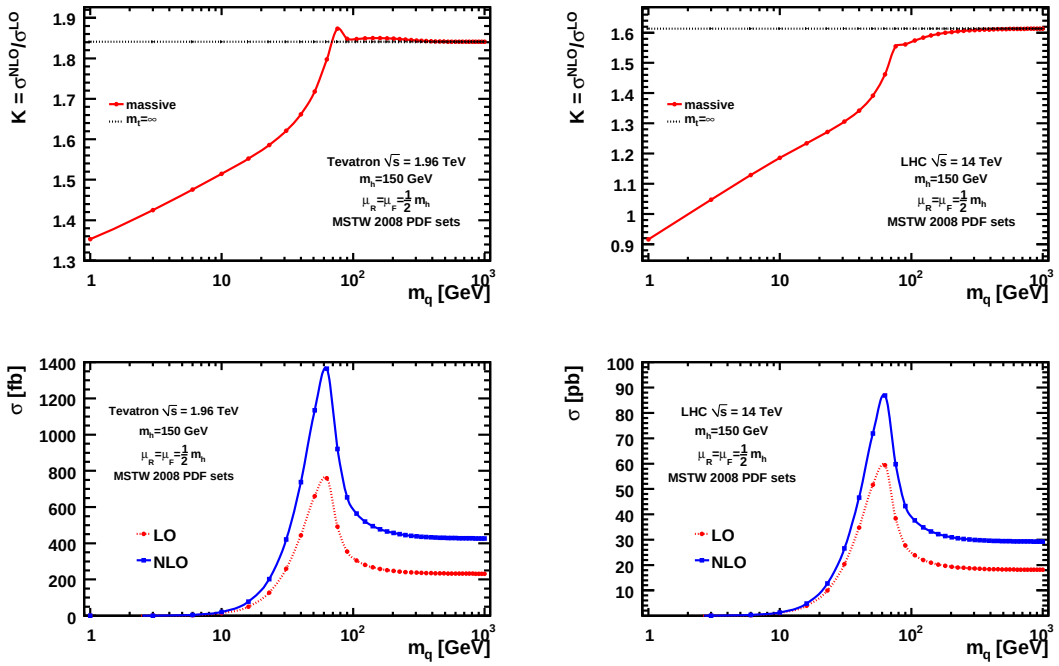

Figure 4. NLO cross-section and K-factor for the gluon fusion process via one only heavy quark at the Tevatron and the LHC, as a function of the quark mass.

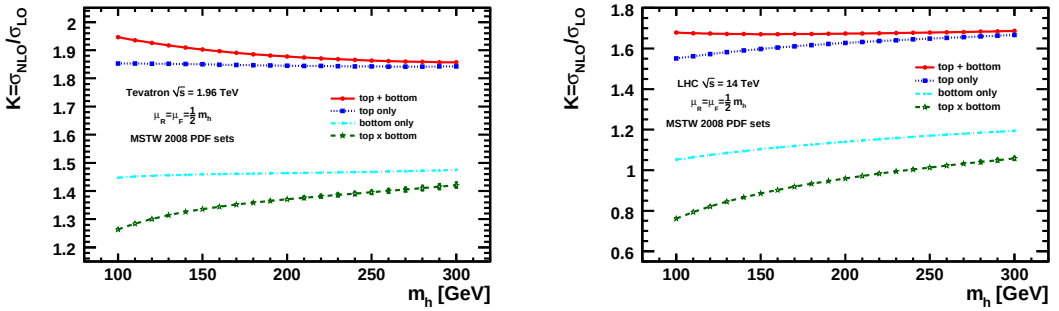

Figure 5. NLO K-factors for the top-only, bottom-only, and top-bottom interference contributions. We restrict to a range of $m_{\rm H}$ where top-bottom interference contributions are still sizable.

cross-section for the gluon fusion cross-section at the Tevatron and the LHC, considering only one heavy quark with a mass m_q. We find that, in the pole scheme, the K-factor is reduced significantly for small values of the quark mass consistent with neglecting the running of the quark mass in the Higgs coupling at leading order.

For the Standard Model where both top and bottom quark loops contribute to the gluon fusion process, we study separately the magnitude of QCD corrections for the top-only, bottom-only, and top-bottom interference terms. The corresponding K-factors at NLO are plotted in figure 5. While the top-only contributions receive a large K-factor, NLO QCD corrections to the top-bottom interference and bottom-only terms are milder. As a consequence, the importance of the bottom-quark loops is smaller at NLO than at LO.

JHEP10(2009)068

The small NLO QCD corrections to the top-bottom interference contribution, which is also a very small fraction of the top-only contribution, suggests that a more precise evaluation at NNLO is not necessary. The top-only contribution receives however large NLO corrections and it requires an evaluation at NNLO. As shown in figure 2, this contribution can be approximated using eq. 3.1 better than 2% for a light Higgs boson, and better than 10% for a Higgs boson with a mass above the top-pair threshold. It appears to us, that the combination of the NLO cross-section with full dependence on the top and bottom quark masses and the NNLO correction using the approximation of eq. 3.1 yields a very precise estimate of the gluon fusion cross-section, where differences with an NNLO calculation with exact finite quark mass effects should be quite small.

The results of this section have been extensively cross-checked with `HIGLU` and excellent agreement has been found.

4 Differential cross-sections at NLO with finite quark masses

The search for a Higgs boson at hadron colliders is complicated due to the large cross-sections of background processes. Sophisticated experimental analyses are required, where it is essential to find optimized selection cuts. In addition, it is often necessary to perform a detailed probabilistic comparison of measured shapes for kinematic distributions with theoretical predictions for the signal and background processes. The role of very accurate Monte-Carlo programs which are fully differential is very important for these purposes.

The fully differential NNLO Monte-Carlo's, `FEHiP` [7–9] and `HNNLO` [10, 11], are available for the gluon fusion Higgs boson production process. Given the complexity of NNLO computations, these programs employ the approximation of eq. 3.1. In some cases, experimental cuts lead to a significantly smaller scale variation than in the total cross-section. This enhances the importance of other uncertainties, such as the one due to unaccounted finite quark mass effects. A characteristic example is the accepted cross-section for $pp \to H \to WW \to ll\nu\nu$ where a jet-veto and other cuts reduce the uncertainty due to scale variations by a factor of about two with respect to the total cross-section [9, 11, 28].

With our exact NLO Monte-Carlo `HPro`, we can correct the predictions of `FEHiP` and `HNNLO` for finite quark mass effects through NLO. `HPro` can be used to compute fully differential cross-sections and distributions at NLO for the Higgs boson and the final state particles in the two photon and four lepton decays. `HPro` is merged with the `FEHiP` NNLO Monte-Carlo and it will be released in a forthcoming publication. In this section, we illustrate the shapes of a few kinematic distributions with our new `HPro` NLO Monte-Carlo and compare them with the corresponding predictions in the "$m_{\rm top} = \infty$" approximation.

In figures 6 and 7, we study the normalized NLO rapidity distribution of a Higgs boson with mass $m_{\rm H} = 150\,\text{GeV}$ at the LHC and the Tevatron, respectively. Except for very large rapidities, where almost no events occur, the distribution is not affected by mass effects. Even in that range the deviations from the "$m_{\rm top} = \infty$" limit are less than 5% at the LHC and less than 10% at the Tevatron. We conclude that small-x effects are moderate and without phenomenological consequences in the case of the rapidity distribution at NLO shedding light on an open question raised in [26, 27].

JHEP10(2009)068

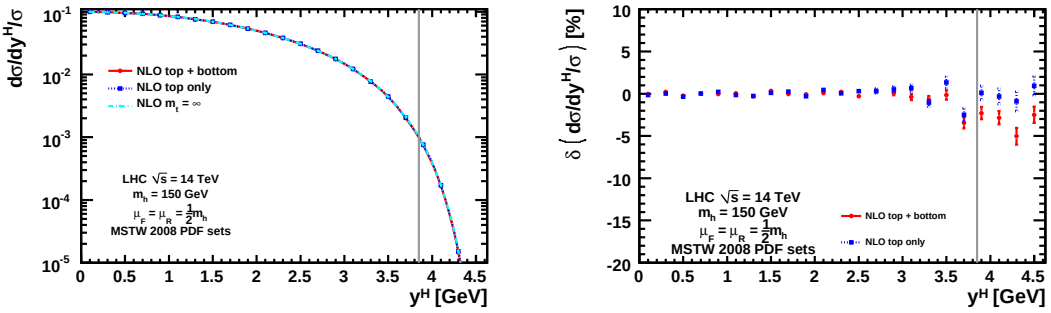

Figure 6. NLO normalized rapidity distribution at the LHC, $m_{\rm H} = 150\,\text{GeV}$. Finite quark mass effects affect the shape of the distributions only in the very high rapidity range, where only a tiny fraction of events take place. For $y^{\rm H}$ values larger than the one marked by the grey line, less than 10^{-3} of the total number of events take place.

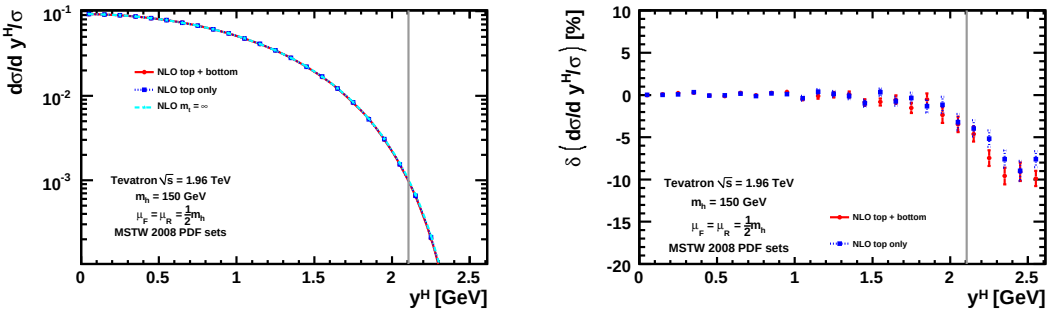

Figure 7. NLO normalized rapidity distribution at the Tevatron, $m_{\rm H} = 150\,\text{GeV}$. Finite quark mass effects affect the shape of the distributions only in the very high rapidity range, where only a tiny fraction of events take place. For $y^{\rm H}$ values larger than the one marked by the grey line, less than 10^{-3} of the total number of events take place.

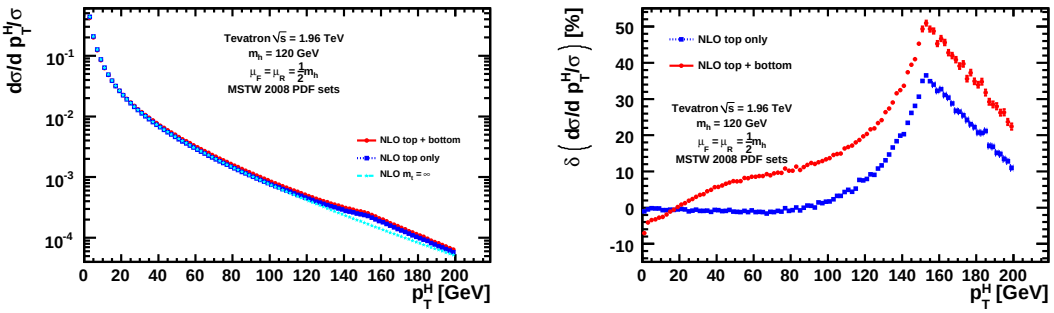

Figure 8. Normalized $p_{\rm T}$ distribution at Tevatron, $m_{\rm H} = 120\,\text{GeV}$. Massive corrections are important for large $p_{\rm T}$. However only a very small fraction of events exists in this range.

Another important differential distribution is the transverse momentum of the Higgs boson. Finite quark mass effects for the $p_{\rm T}$ distribution have also been studied in earlier publications [18, 19, 25], and recently both electroweak and finite quark mass corrections were computed and combined [20].

JHEP10(2009)068

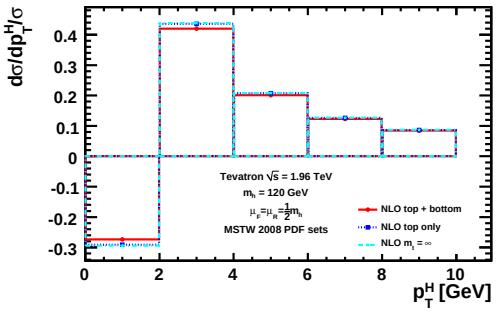

Figure 9. First few bins of $p_{\rm T}$ distribution at Tevatron, $m_{\rm H} = 120\,\text{GeV}$. The values of these bins are unphysical and require resummation.

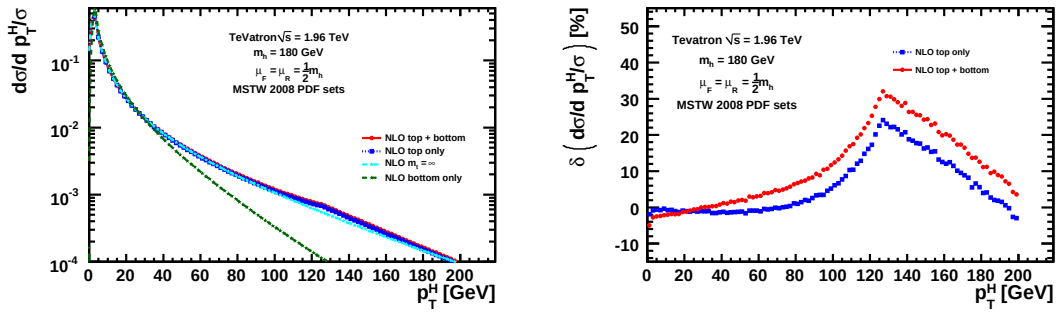

Figure 10. Normalized $p_{\rm T}$ distribution at Tevatron, $m_{\rm H} = 180\,\text{GeV}$. Compared to $m_{\rm H} = 120\,\text{GeV}$, mass corrections lead to smaller deviations from the "$m_{\rm top} = \infty$" approximation. The spectrum of the bottom-only contribution is much softer (green, left panel).

In figure 8 (left panel) we present the normalized cross-section at the Tevatron in $p_{\rm T}$ bins of 2 GeV, for a Higgs boson with mass $m_{\rm H} = 120\,\text{GeV}$. At small values of $p_{\rm T}$ the bin cross-sections cannot be computed accurately in perturbation theory, see figure 9, and an all orders resummation is required [29, 30]. A meaningful result is obtained, however, when the bins at low $p_{\rm T}$ are added up together. In order to study the effect of finite quark masses it is more convenient if we demonstrate uncombined low $p_{\rm T}$ bins. For this purpose, we present the $p_{\rm T}$ distribution in the approximation of eq. 3.1 (cyan), in the "top-only" approximation (blue) where the bottom loops are ignored but the top-loops are evaluated exactly, and with the complete "top-bottom" mass dependence (red). We have compared our results with the authors of [20] and found full agreement within numerical errors. In the right panel of figure 8 we show the percent deviations of the complete result (red) and the "top-only" approximation for the normalized $p_{\rm T}$ distribution from the approximation of eq. 3.1. At small $p_{\rm T}$, there are very small differences due to finite quark-mass effects. We observe some important shape deviations due to the effect of top and bottom quark loops at intermediate $p_{\rm T}$. As it has already been observed in ref. [20] finite quark effects are very large at high $p_{\rm T}$, where the quark production channel becomes dominant. Note that additional electroweak corrections affect the shape considerably [20]. At a higher Higgs boson mass value of $m_{\rm H} = 180\,\text{GeV}$ (figure 10) we find an even milder effect at low $p_{\rm T}$,

JHEP10(2009)068

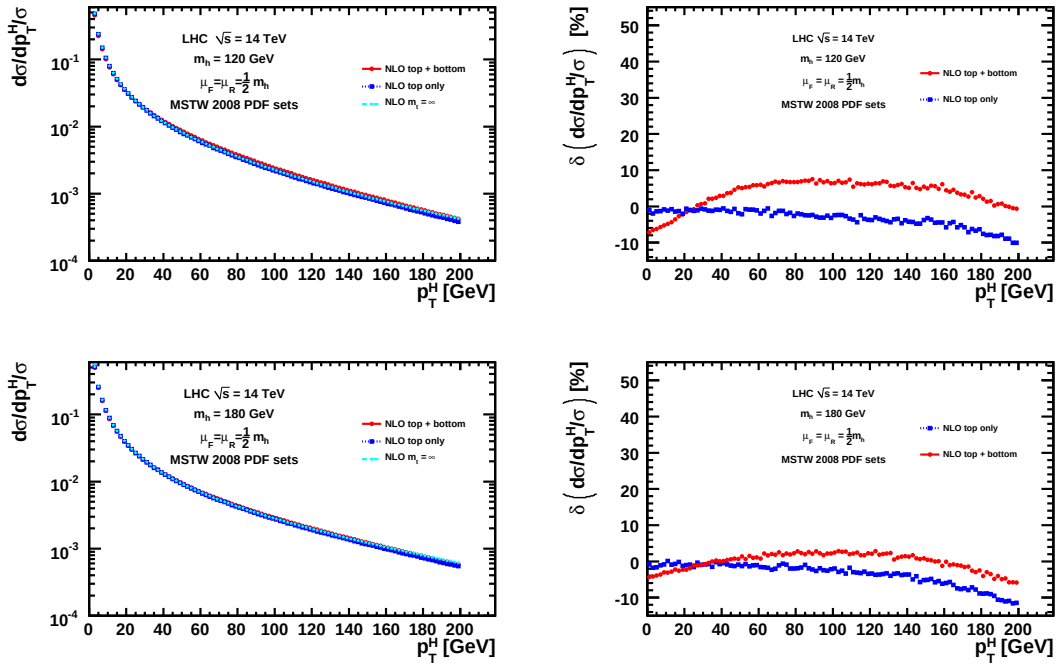

Figure 11. Normalized $p_{\rm T}$ distribution at LHC for $m_{\rm H} = 120\,{\rm GeV}$ and $m_{\rm H} = 180\,{\rm GeV}$. Mass corrections are much more modest than at Tevatron where the $q\bar{q}$ channel plays a much bigger rôle.

while the magnitude of the deviations at a large $p_{\rm T}$ is somewhat reduced but still large. For phenomenological purposes, these large deviations concern a tiny fraction of potential Higgs signal events for both $m_{\rm H} = 120\,{\rm GeV}$ and $m_{\rm H} = 180\,{\rm GeV}$ mass values. We show in figure 10 also the "bottom-only" contribution and observe that in this case the $p_{\rm T}$ spectrum is much softer, as pointed out in ref. [25].

At LHC energy (14 TeV), figure 11, we observe significant bottom-loop effects for a light Higgs boson ($m_{\rm H} = 120\,{\rm GeV}$). These are reduced, for a heavier Higgs boson with mass $m_{\rm H} = 180\,{\rm GeV}$. Shape deviations due to finite quark mass effects can reach up to 10% at high $p_{\rm T}$. It is interesting that bottom quark loops for a light Higgs boson change the shape at low $p_{\rm T}$. As we explained, the fixed order $p_{\rm T}$ spectrum is not physical at low $p_{\rm T}$. However, these deviations may also survive after a complete resummation is performed via the matching procedure. It is interesting to examine the $p_{\rm T}$ spectrum for a Higgs mass where the heavy top approximation is formally invalid. In figure 12 we plot the normalized distribution for $m_{\rm H} = 400\,{\rm GeV}$ at the LHC. Deviations of the "top-only" contributions from the infinitely heavy top-quark approximation are small for $p_{\rm T} < 80\,{\rm GeV}$. At higher $p_{\rm T}$ the difference increases.

Finally, we present normalized distributions for Higgs decay final state. In figure 13 we present the pseudorapidity difference and average $p_{\rm T}$ distribution of the two photons in the process $pp \to H \to \gamma\gamma$. Finite quark-mass effects do not affect these distributions. At higher Higgs boson masses the process $pp \to H \to WW \to ll\nu\nu$ is dominating and we show as an example for this decay mode the ϕ_{ll} distribution in figure 14. ϕ_{ll} is the angle in the transverse plane between the two charged leptons in the final state and we find again, that the shape is very well reproduced by the "$m_{\rm top} = \infty$" approximation.

JHEP10(2009)068

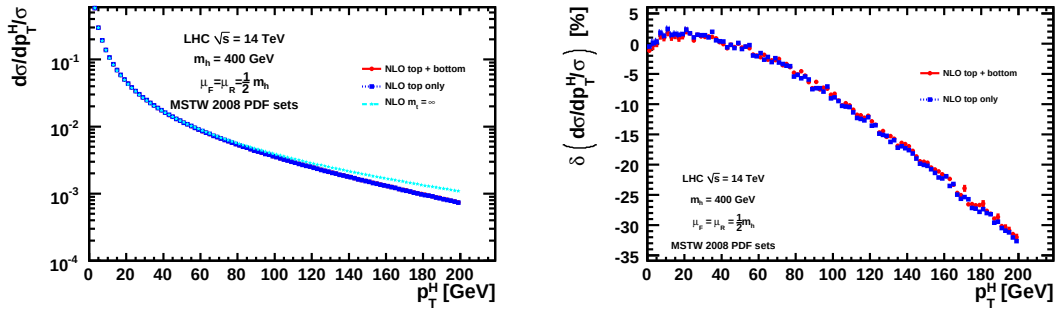

Figure 12. Normalized p_{T} distribtution at LHC for $m_{\mathrm{H}} = 400\,\mathrm{GeV}$. Mass effects become important as $m_{\mathrm{top}} = \infty$ approximation is formally invalid.

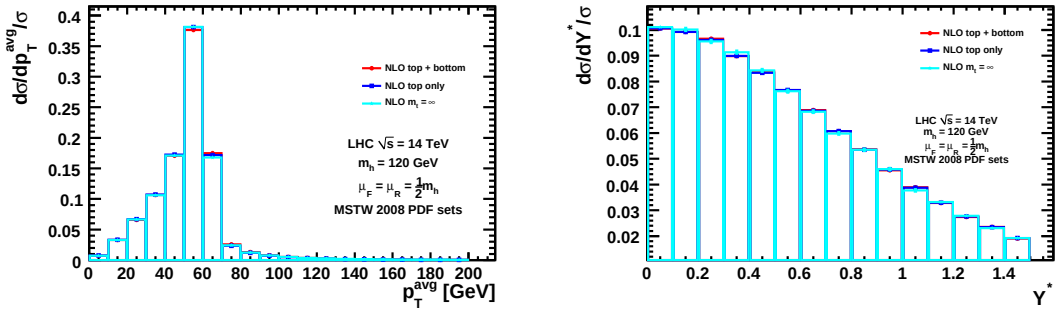

Figure 13. On the left: Normalized distribution of the average photon transverse momentum, ${p_{\mathrm{T}}}^{\mathrm{avg}} = ({p_{\mathrm{T}}}^{\gamma_1} + {p_{\mathrm{T}}}^{\gamma_2})/2$. On the right: Normalized distribution of photon pseudorapidity difference, $Y^* = |\eta^{\gamma_1} - \eta^{\gamma_2}|/2$. In both plots $m_{\mathrm{H}} = 120\,\mathrm{GeV}$ and we assume LHC energies.

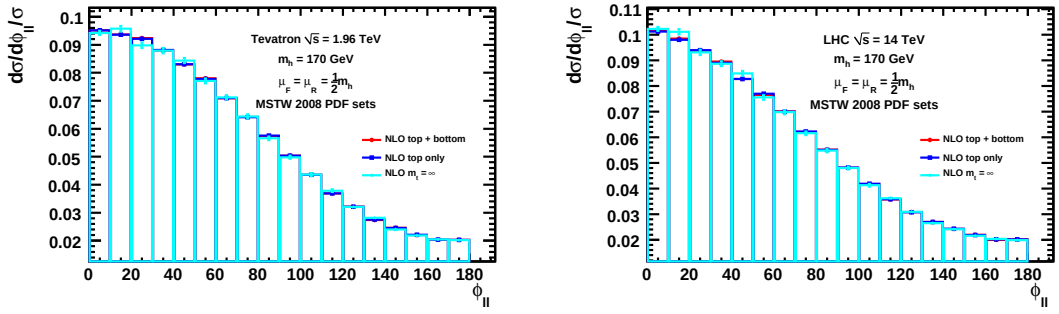

Figure 14. Normalized ϕ_{ll} distribution for $m_{\mathrm{H}} = 170\,\mathrm{GeV}$ at Tevatron and LHC. ϕ_{ll} is the angle in the transverse plane between the charged final state leptons, $\phi_{ll} = (p_\perp^{l_1} \cdot p_\perp^{l_2})/|p_\perp^{l_1}||p_\perp^{l_2}|$.

In summary, we have found that the shapes of distributions for leptons and photons from the decay of a Higgs boson are very well approximated by eq. 3.1. In addition, accepted cross-sections after the application of cuts on jets are affected consistently with the expectations from the shapes of the Higgs p_{T} spectra.

JHEP10(2009)068

5 Conclusions

In this paper, we have presented a NLO partonic level Monte-Carlo program `HPro`, which computes the top and bottom quark mass dependence of differential cross-sections exactly. `HPro` computes accepted cross-sections after selection cuts and kinematic distributions for final-state particles in the diphoton and four-lepton decay channels.

Finite quark mass effects are important and can affect the precision of NNLO calculations in the infinite top-quark mass approximation. We can use `HPro` to correct NNLO differential cross-sections for finite quark mass effects. For this purpose, we have interfaced `HPro` with the fully exclusive NNLO Monte-Carlo `FEHiP`. The combined program will be released in a forthcoming publication.

Acknowledgments

We thank Frank Petriello for useful discussions and comparisons. We are grateful to Alejandro Daleo for a stimulating collaboration at early stages of this work. This work was supported by the Swiss National Science Foundation under contract 200021-117873.

A Real radiation matrix elements

Here we present the results for the matrix elements squared for real radiation processes $gg \to gh$, $qg \to qh$ and $q\bar{q} \to gh$ in terms of helicity amplitudes. We introduce the following shorthand notation for scalar one-loop integrals,

$$\mathrm{B}\,(s,m) = -\mathrm{i}(4\pi)^2 B_0^{\mathrm{fin}}(s;m)\,, \tag{A.1}$$

$$\mathrm{C}\,(s,m) = -\mathrm{i}(4\pi)^2 C_0(0,0,s;m,m,m)\,, \tag{A.2}$$

$$\mathrm{C}_1\,(s,t,m) = -\mathrm{i}(4\pi)^2 C_0(0,s,t;m,m,m)\,, \tag{A.3}$$

$$\mathrm{D}\,(s,t,m) = -\mathrm{i}(4\pi)^2 D_0(0,0,0,m_H^2,s,t;m,m,m,m) \tag{A.4}$$

where B_0, C_0 and D_0 are the standard one-loop integrals in the notation of e.g. [31]. B_0^{fin} is the finite part of the B_0 function, i.e.

$$B_0(s;m) = \frac{\mathrm{i}}{(4\pi)^2}\left(\frac{1}{\epsilon} + B_0^{\mathrm{fin}}(s;m)\right)\,. \tag{A.5}$$

There exist several publicly available packages for evaluating one-loop integrals [31–33]. However, we used a private implementation and checked against these packages.

In the following we present the real radiation matrix elements squared, averaged over spin and color and divided by the flux factor, in terms of helicity amplitudes, closely adapting the notation in [19]. Note however the different convention regarding helicity labels. The simplest process is $q\bar{q} \to gh$ and the result can be expressed by a single independent helicity amplitude,

$$\Upsilon^r_{q\bar{q}}(s_{12},s_{13},s_{23}) = \frac{{\alpha_s}^3(N_c^2-1)}{16\pi N_c^2 s_{12}^2}\left(\Big|\sum_Q M_Q^{q\bar{q}}(s_{12},s_{13},s_{23})\Big|^2 + \Big|\sum_Q M_Q^{q\bar{q}}(s_{12},s_{23},s_{13})\Big|^2\right). \tag{A.6}$$

with

$$M_Q^{q\bar{q}}(s_{12},s_{13},s_{23}) = \frac{\Lambda_Q m_Q^2 s_{23}}{s_{23}+s_{13}}\Big[2(s_{13}+s_{23}-4m_Q^2)\mathrm{C}_1\left(m_H^2,s_{12},m_Q\right) + \frac{4s_{12}}{s_{23}+s_{13}}\left(\mathrm{B}\left(s_{12},m_Q\right)-\mathrm{B}\left(m_H^2,m_Q\right)\right)-4\Big]. \tag{A.7}$$

Here, $m_Q\Lambda_Q$ ($\Lambda_Q = 1/v$), is the Higgs-quark-quark coupling and we sum over heavy quarks, $Q = t, b$.

Similarly simple is the result for $qg \to qh$ and $gq \to qh$ sub-processes which is obtained by crossing,

$$\Upsilon^r_{qg}(s_{12},s_{13},s_{23}) = -\frac{N_c}{N_c^2-1}\Upsilon^r_{q\bar{q}}(s_{23},s_{13},s_{12}), \tag{A.8}$$

$$\Upsilon^r_{gq}(s_{12},s_{13},s_{23}) = -\frac{N_c}{N_c^2-1}\Upsilon^r_{q\bar{q}}(s_{13},s_{12},s_{23}). \tag{A.9}$$

More involved is the expression for the $gg \to gh$ process. However, it has a compact representation in terms of only two independent helicity amplitudes,

$$\Upsilon^r_{gg}(s_{12},s_{13},s_{23}) = \frac{{\alpha_s}^3 N_c}{8\pi(N_c^2-1)s_{12}^2 s_{13}s_{23}}\times \tag{A.10}$$
$$\times\Big(\Big|\sum_Q M^{gg}_{Q;++-}(s_{12},s_{13},s_{23})\Big|^2+\Big|\sum_Q M^{gg}_{Q;++-}(s_{13},s_{12},s_{23})\Big|^2 + \Big|\sum_Q M^{gg}_{Q;++-}(s_{23},s_{13},s_{12})\Big|^2+\Big|\sum_Q M^{gg}_{Q;+++}(s_{12},s_{13},s_{23})\Big|^2\Big).$$

The amplitudes appearing in this expression are given by

$$\begin{aligned}
M^{gg}_{Q;++-}(s_{12},s_{13},s_{23}) = \Lambda_Q m_Q^2\Big[& -\frac{4s_{12}({s_{12}}^2-s_{13}s_{23})}{(s_{23}+s_{12})(s_{13}+s_{12})} \\
& -\frac{1}{2}\frac{s_{12}s_{23}(4m_Q^2 s_{13}-s_{12}s_{13})}{s_{13}}\mathrm{D}\left(s_{12},s_{23},m_Q\right) \\
& -\frac{1}{2}\frac{s_{12}s_{13}(4s_{23}m_Q^2-s_{12}s_{23})}{s_{23}}\mathrm{D}\left(s_{13},s_{12},m_Q\right) \\
& +\frac{1}{2}\frac{s_{23}s_{13}(-{s_{12}}^2+12s_{12}m_Q^2+4s_{13}s_{23})}{s_{12}}\mathrm{D}\left(s_{13},s_{23},m_Q\right) \\
& -\frac{4s_{13}(2s_{12}s_{23}+{s_{23}}^2)}{(s_{23}+s_{12})^2}\mathrm{B}\left(s_{13},m_Q\right)-\frac{4s_{23}(2s_{12}s_{13}+{s_{13}}^2)}{(s_{13}+s_{12})^2}\mathrm{B}\left(s_{23},m_Q\right) \\
& -\frac{2s_{13}s_{23}}{(s_{13}+s_{12})^2(s_{23}+s_{12})^2}\Big(-4{s_{13}}^2s_{12}-2s_{23}{s_{13}}^2-8s_{13}s_{12}s_{23} \\
& -10s_{13}{s_{12}}^2-2{s_{23}}^2s_{13}-10s_{23}{s_{12}}^2-4s_{12}{s_{23}}^2-8{s_{12}}^3\Big)\mathrm{B}\left(m_H^2,m_Q\right) \\
& +\frac{(s_{13}s_{12}s_{23}-4s_{13}s_{23}m_Q^2)(s_{23}+s_{13})}{s_{13}s_{23}}\mathrm{C}_1\left(m_H^2,s_{12},m_Q\right) \\
& +\frac{1}{(s_{23}+s_{12})}(4s_{13}{s_{23}}^2-s_{12}{s_{23}}^2+2\frac{{s_{23}}^3s_{13}}{s_{12}}+2s_{13}s_{23}s_{12}+{s_{12}}^3
\end{aligned} \tag{A.11}$$

$$
\begin{aligned}
&+ 4m_Q^2({s_{23}}^2 + 2s_{12}s_{23} - {s_{12}}^2))\mathrm{C}_1\left(m_H^2, s_{13}, m_Q\right) \\
&+ \frac{1}{(s_{13}+s_{12})}(4s_{23}{s_{13}}^2 - s_{12}{s_{13}}^2 + 2\frac{{s_{13}}^3 s_{23}}{s_{12}} + 2s_{23}s_{13}s_{12} + {s_{12}}^3 \\
&+ 4m_Q^2({s_{13}}^2 + 2s_{12}s_{13} - {s_{12}}^2))\mathrm{C}_1\left(m_H^2, s_{23}, m_Q\right) \\
&- 2\frac{{s_{13}}^2 s_{23}}{s_{12}}\mathrm{C}\left(s_{13}, m_Q\right) - 2\frac{{s_{23}}^2 s_{13}}{s_{12}}\mathrm{C}\left(s_{23}, m_Q\right)\Bigg]
\end{aligned}
$$

and

$$
\begin{aligned}
M^{gg}_{Q;+++}(s_{12}, s_{13}, s_{23}) = \Lambda_Q m_Q^2\Bigg[&- 4(s_{13}+s_{23}+s_{12}) \\
&- \frac{1}{2}\frac{s_{23}s_{12}(4m_Q^2 s_{13} - s_{13}s_{23} - s_{12}s_{13} - {s_{13}}^2)}{s_{13}}\mathrm{D}\left(s_{12}, s_{23}, m_Q\right) \\
&- \frac{1}{2}\frac{s_{12}s_{13}(4s_{23}m_Q^2 - s_{12}s_{23} - s_{13}s_{23} - {s_{23}}^2)}{s_{23}}\mathrm{D}\left(s_{13}, s_{12}, m_Q\right) \\
&- \frac{1}{2}\frac{s_{23}s_{13}(4s_{12}m_Q^2 - s_{12}s_{23} - {s_{12}}^2 - s_{12}s_{13})}{s_{12}}\mathrm{D}\left(s_{13}, s_{23}, m_Q\right) \\
&+ \frac{(s_{13}s_{12}s_{23} + s_{13}{s_{23}}^2 + {s_{13}}^2 s_{23} - 4s_{13}s_{23}m_Q^2)(s_{23}+s_{13})}{s_{23}s_{13}}\mathrm{C}_1\left(m_H^2, s_{12}, m_Q\right) \\
&+ \frac{(s_{12}{s_{23}}^2 + {s_{12}}^2 s_{23} + s_{13}s_{12}s_{23} - 4s_{12}s_{23}m_Q^2)(s_{23}+s_{12})}{s_{12}s_{23}}\mathrm{C}_1\left(m_H^2, s_{13}, m_Q\right) \\
&+ \frac{({s_{12}}^2 s_{13} - 4s_{12}m_Q^2 s_{13} + s_{13}s_{12}s_{23} + s_{12}{s_{13}}^2)(s_{13}+s_{12})}{s_{12}s_{13}}\mathrm{C}_1\left(m_H^2, s_{23}, m_Q\right)\Bigg].
\end{aligned}
\tag{A.12}
$$

References

[1] A. Djouadi, M. Spira and P.M. Zerwas, *Production of Higgs bosons in proton colliders: QCD corrections*, *Phys. Lett.* **B 264** (1991) 440 [SPIRES].

[2] S. Dawson, *Radiative corrections to Higgs boson production*, *Nucl. Phys.* **B 359** (1991) 283 [SPIRES].

[3] M. Spira, A. Djouadi, D. Graudenz and P.M. Zerwas, *Higgs boson production at the LHC*, *Nucl. Phys.* **B 453** (1995) 17 [hep-ph/9504378] [SPIRES].

[4] R.V. Harlander and W.B. Kilgore, *Next-to-Next-to-Leading order Higgs production at hadron colliders*, *Phys. Rev. Lett.* **88** (2002) 201801 [hep-ph/0201206] [SPIRES].

[5] C. Anastasiou and K. Melnikov, *Higgs boson production at hadron colliders in NNLO QCD*, *Nucl. Phys.* **B 646** (2002) 220 [hep-ph/0207004] [SPIRES].

[6] V. Ravindran, J. Smith and W.L. van Neerven, *NNLO corrections to the total cross section for Higgs boson production in hadron hadron collisions*, *Nucl. Phys.* **B 665** (2003) 325 [hep-ph/0302135] [SPIRES].

[7] C. Anastasiou, K. Melnikov and F. Petriello, *Higgs boson production at hadron colliders: differential cross sections through Next-to-Next-to-Leading order*, *Phys. Rev. Lett.* **93** (2004) 262002 [hep-ph/0409088] [SPIRES].

JHEP10(2009)068

[8] C. Anastasiou, K. Melnikov and F. Petriello, *Fully differential Higgs boson production and the di- photon signal through Next-to-Next-to-Leading order*, *Nucl. Phys.* **B 724** (2005) 197 [hep-ph/0501130] [SPIRES].

[9] C. Anastasiou, G. Dissertori and F. Stockli, *NNLO QCD predictions for the $H \to WW \to ll\nu\nu$ signal at the LHC*, *JHEP* **09** (2007) 018 [arXiv:0707.2373] [SPIRES].

[10] S. Catani and M. Grazzini, *An NNLO subtraction formalism in hadron collisions and its application to Higgs boson production at the LHC*, *Phys. Rev. Lett.* **98** (2007) 222002 [hep-ph/0703012] [SPIRES].

[11] M. Grazzini, *NNLO predictions for the Higgs boson signal in the $H \to WW \to \nu l\nu$ and $H \to ZZ \to 4l$ decay channels*, *JHEP* **02** (2008) 043 [arXiv:0801.3232] [SPIRES].

[12] M. Spira, *HIGLU and HDECAY: programs for Higgs boson production at the LHC and Higgs boson decay widths*, *Nucl. Instrum. Meth.* **A 389** (1997) 357 [hep-ph/9610350] [SPIRES].

[13] C. Anastasiou, R. Boughezal and F. Petriello, *Mixed QCD-electroweak corrections to Higgs boson production in gluon fusion*, *JHEP* **04** (2009) 003 [arXiv:0811.3458] [SPIRES].

[14] D. de Florian and M. Grazzini, *Higgs production through gluon fusion: updated cross sections at the Tevatron and the LHC*, *Phys. Lett.* **B 674** (2009) 291 [arXiv:0901.2427] [SPIRES].

[15] R. Harlander and P. Kant, *Higgs production and decay: analytic results at Next-to-Leading Order QCD*, *JHEP* **12** (2005) 015 [hep-ph/0509189] [SPIRES].

[16] C. Anastasiou, S. Beerli, S. Bucherer, A. Daleo and Z. Kunszt, *Two-loop amplitudes and master integrals for the production of a Higgs boson via a massive quark and a scalar-quark loop*, *JHEP* **01** (2007) 082 [hep-ph/0611236] [SPIRES].

[17] U. Aglietti, R. Bonciani, G. Degrassi and A. Vicini, *Analytic results for virtual QCD corrections to Higgs production and decay*, *JHEP* **01** (2007) 021 [hep-ph/0611266] [SPIRES].

[18] R.K. Ellis, I. Hinchliffe, M. Soldate and J.J. van der Bij, *Higgs decay to $\tau^+\tau^-$: a possible signature of intermediate mass Higgs bosons at the SSC*, *Nucl. Phys.* **B 297** (1988) 221 [SPIRES].

[19] U. Baur and E.W.N. Glover, *Higgs boson production at large transverse momentum in hadronic collisions*, *Nucl. Phys.* **B 339** (1990) 38 [SPIRES].

[20] W.-Y. Keung and F.J. Petriello, *Electroweak and finite quark-mass effects on the Higgs boson transverse momentum distribution*, *Phys. Rev.* **D 80** (2009) 013007 [arXiv:0905.2775] [SPIRES].

[21] S. Frixione, Z. Kunszt and A. Signer, *Three jet cross-sections to Next-to-Leading Order*, *Nucl. Phys.* **B 467** (1996) 399 [hep-ph/9512328] [SPIRES].

[22] S. Alioli, P. Nason, C. Oleari and E. Re, *NLO Higgs boson production via gluon fusion matched with shower in POWHEG*, *JHEP* **04** (2009) 002 [arXiv:0812.0578] [SPIRES].

[23] T. Hahn, *CUBA: a library for multidimensional numerical integration*, *Comput. Phys. Commun.* **168** (2005) 78 [hep-ph/0404043] [SPIRES].

[24] A.D. Martin, W.J. Stirling, R.S. Thorne and G. Watt, *Parton distributions for the LHC*, *Eur. Phys. J.* **C 63** (2009) 189 [arXiv:0901.0002] [SPIRES].

[25] U. Langenegger, M. Spira, A. Starodumov and P. Trueb, *SM and MSSM Higgs boson production: spectra at large transverse momentum*, *JHEP* **06** (2006) 035 [hep-ph/0604156] [SPIRES].

JHEP10(2009)068

[26] S. Marzani, R.D. Ball, V. Del Duca, S. Forte and A. Vicini, *Higgs production via gluon-gluon fusion with finite top mass beyond Next-to-Leading Order*, *Nucl. Phys.* **B 800** (2008) 127 [arXiv:0801.2544] [SPIRES].

[27] S. Marzani, R.D. Ball, V. Del Duca, S. Forte and A. Vicini, *Finite-top-mass effects in NNLO Higgs production*, *Nucl. Phys. Proc. Suppl.* **186** (2009) 98 [arXiv:0809.4934] [SPIRES].

[28] C. Anastasiou, G. Dissertori, M. Grazzini, F. Stockli and B.R. Webber, *Perturbative QCD effects and the search for a $H \to WW \to l\nu l\nu$ signal at the Tevatron*, *JHEP* **08** (2009) 099 [arXiv:0905.3529] [SPIRES].

[29] G. Bozzi, S. Catani, D. de Florian and M. Grazzini, *The $q(T)$ spectrum of the Higgs boson at the LHC in QCD perturbation theory*, *Phys. Lett.* **B 564** (2003) 65 [hep-ph/0302104] [SPIRES].

[30] S. Frixione and B.R. Webber, *Matching NLO QCD computations and parton shower simulations*, *JHEP* **06** (2002) 029 [hep-ph/0204244] [SPIRES]; *The MC@NLO3.4 event generator*, arXiv:0812.0770 [SPIRES].

[31] T. Hahn and M. Pérez-Victoria, *Automatized one-loop calculations in four and D dimensions*, *Comput. Phys. Commun.* **118** (1999) 153 [hep-ph/9807565] [SPIRES].

[32] G.J. van Oldenborgh, *FF: a package to evaluate one loop Feynman diagrams*, *Comput. Phys. Commun.* **66** (1991) 1 [SPIRES].

[33] R.K. Ellis and G. Zanderighi, *Scalar one-loop integrals for QCD*, *JHEP* **02** (2008) 002 [arXiv:0712.1851] [SPIRES].

JHEP10(2009)068